Linking selection to demography in experimental evolution of active death in a unicellular organism

Running title: Selection on population decline

Nathalie Zeballos[1], Océane Rieu[1,2], Stanislas Fereol[1], Christelle Leung[1], and Luis-Miguel Chevin[1]

[1] CEFE, Université de Montpellier, CNRS, EPHE, IRD, Montpellier, France

[2] MIVEGEC, Université de Montpellier, CNRS, IRD, Montpellier, France

Correspondence : Nathalie Zeballos

Email : nathalie.zeballos@gmail.com, nathalie.zeballos@cefe.cnrs.fr,

Keywords: population decline, natural selection, competition, experimental evolution, environmental stress, programmed cell death.

The number of figures, tables: 5 figures and 1 table

Statement of Authorship: NZ, CL and L-MC conceived and designed the study. NZ, SF and OR performed the experiments and collected the data. NZ and L-MC build the estimation frequency method. NZ analysed the data, prepared figures and tables, and wrote the original draft, CL and L-MC reviewed and edited the draft. All the authors reviewed and approved the final draft of the manuscript.

Data accessibility statement: Data and code that support the findings of this study are archived in a zenodo repository (DOI : 10.5281/zenodo.12580685).

Abstract:

Deciphering how natural selection emerges from demographic differences among genotypes, and reciprocally how evolution affects population dynamics, is key to understanding population responses to environment stress, especially in non-trivial ecological scenarios. Many microbes can trigger programmed cell death (PCD) in response to stress, causing massive population decline followed by rapid rebound. To understand how selection may operate on this trait, we exposed monocultures and mixtures of two closely related strains of the microalga *Dunalliela salina* that do or do not induce PCD to multiple cycles of hyper-osmotic shock, and tracked demography and selection throughout. Population dynamics in mixtures and monocultures were largely consistent, suggesting that strong ecological interactions do not drive selection on PCD during the decline-rebound phase. Instead, long-term coexistence was largely explained by density-dependent competition near the stationary phase, regardless of the large frequency fluctuations at each cycle induced by the decline-rebound dynamics.

Introduction

Natural selection is intrinsically a demographic process, arising from the differential growths of genotypes with different vital rates (survival and fecundity), causing variation in fitness (Charles 1859; Crow & Kimura 1970). However beyond this uncontroversial statement, deducing selection from demographic properties often proves a non-trivial effort, as exemplified by the difficulty in finding a universally satisfying definition of fitness (De Jong 1994; Lenormand, T., Rode, N., Chevin, L. M., & Rousset 2016). One of the most common practical issues when trying to relate selection to demography involves finding out to what extent absolute fitness of genotypes measured in isolation can be used to predict selection when these genotypes are in competition (Chevin 2011).

It is well understood that what matters for selection and evolution is relative fitness, the difference between the relative growth rates of different types in competition (Crow & Kimura 1970; Lenski 1991; Lenski *et al.* 1997). However, measuring relative fitness comes with the technical challenge of being able to distinguish the competing genotypes. This can be achieved by relying on natural phenotypic variation such as color polymorphism (Cain & Sheppard 1954; Fisher R. A. & Ford E. B. 1947); by inserting phenotypic markers such as fluorescent proteins (Gallet *et al.* 2012); or by sequencing standing genetic variants (Burke *et al.* 2010; Burny *et al.* 2022; Rescan *et al.* 2021), or designed 'barcode' sequences (Levy *et al.* 2015). Beyond these technical limitations, focusing solely on relative fitness can make it difficult to decipher the causes and mechanisms of selection across environments and ecological contexts. More insight may be obtained by studying the demographic responses of individual genotypes, and comparing them to their differential growth in competition. Furthermore, focusing solely on relative fitness is clearly insufficient in eco-evolutionary scenarios where the main focus is the evolution of demographic properties of the population (e.g. mean growth rate), for instance during evolutionary rescue (Gomulkiewicz & Holt 1995; Hendry 2017).

Relative fitnesses of competing genotypes can be well predicted from their absolute fitnesses in isolation, provided these genotypes do not interact ecologically in ways that lead to frequency-dependent selection (Chevin 2011; Ribeck & Lenski 2015). This assumption is less likely to hold whenever one of the genotypes excretes beneficial or detrimental substances in the medium (Estrela *et al.* 2019), or benefits from arriving or starting to grow earlier than others (priority effect) (De Meester *et al.* 2016), for instance. Therefore, contexts where these or other forms of ecological interactions are suspected to be important are less likely to show consistency between fitness measured in isolation versus in competition. Reciprocally, finding similar demographic dynamics in isolation and competition can help exclude some forms of interactions between genotypes, and more broadly delineate plausible underlying ecological causes for observed eco-evolutionary dynamics.

We recently showed that two strains of the halotolerant microalga *Dunalliela salina* have drastically different demographic strategies in response to hyper-osmotic stress (Leung *et al.* 2022; Zeballos *et al.* 2023). One of the strains undergoes programmed cell death (hereafter PCD), an active form of cell death that has been reported across a broad range of unicellular organisms in response to a variety of environmental triggers (Ameisen 2002; Bidle 2016; Deponte 2008). In *Dunalliela salina*, the strain inducing PCD undergoes a massive and rapid population decline at the onset of osmotic shock, while a closely related strain does not (Leung *et al.* 2022; Zeballos *et al.* 2023). Strikingly, surviving cells of the declining strain later experience a rebound phase characterized by fast growth, such that their monocultures may reach similar or higher population density than those of the non-declining strain after a few generations (about a week) (Zeballos *et al.* 2023). If these dynamics in monoculture were good predictors of the outcome of competition between these strains, then we would expect the genotype inducing PCD to be favoured by natural selection over successive osmotic shocks,

and thus increase in frequency. This increase in frequency would in turn cause the paradoxical evolution of faster decline in response to hyper-osmotic stress at the population level.

On the other hand, these predictions would be violated if the non-declining strain exhausted resources before the declining strain had recovered from its initial decline, preventing it from rebounding, and leading to competitive exclusion through a priority effect (De Meester *et al.* 2016). Alternatively, dying cells from the declining strain may release resources or cues in the medium that fundamentally modify the growth rate of the co-occurring non-declining strain (Durand *et al.* 2011; Orellana *et al.* 2013). Even regardless of these ecological considerations, the PCD strain can only outgrow its competing strain if it spends enough time in exponential phase during the rebound phase to recover from its initial decline, before reaching a carrying capacity where growth is no longer possible.

To investigate how these processes drive eco-evolutionary dynamics in our system, and better understand the – so far largely misunderstood (Reece *et al.* 2011) - putative benefit of PCD, we exposed monocultures and mixtures of declining and non-declining strains of *D. salina* to 13 cycles of hyper-osmotic stress (~180 generations), and tracked demography and selection throughout. Our results indicate that stable coexistence can arise via density-dependent processes that take place near the stationary phase of growth, largely overriding the influence of complex decline-rebound dynamics caused by PCD.

Materials & Methods

Experimental evolution

We focused on two closely related *Dunalliela salina* strains that were previously shown to differ in their responses to a salinity rise (Leung *et al.* 2022; Zeballos *et al.* 2023). The first one, CCAP 19/12 (hereafter strain A), sharply declines following a rise to very high salinity, as a result of programmed cell death (PCD). This abrupt and massive decline (up to 70-80% of the

population) is then followed by a rapid rebound, characterized by fast population growth. In contrast, the other strain CCAP 19/15 (strain C) does not exhibit any decline-rebound response to salinity rise, instead growing at a relatively constant rate. Our previous investigations of these strains suggested that monocultures of strain A could reach higher density than strain C at the end of the rebound phase (Zeballos *et al.* 2023). We therefore wanted to test whether this is also true in competition, and how this influences experimental evolution of PCD. Both strains were obtained from the Culture Collection of Algae and Protozoan (CCAP) in 2017, and were originally isolated from the same sampling site (North Sinai, Israel). Each of the 10 biological replicates per strain used in this study was founded from a single haploid cell isolated using cells-sorting flow cytometry (BD FACSAria™ IIu; Biosciences-US) in May 2019, ensuring nearly isogenic populations per replicate (but with potential genetic variation among these clones).

To investigate competitive fitness among strains and the resulting experimental evolution of PCD, we exposed several mixtures of these strains to successive osmotic shocks, and tracked their population dynamics and relative frequencies through time. Cell cultures were performed in 50 ml flasks (CELLSTAR®; VWR 392-0016), using custom-made artificial saline water complemented with NaCl (Rescan *et al.* 2020; Zeballos *et al.* 2023). Growth chambers were set to 12h:12h light:dark cycles, with light intensity at 200 $\mu mol.m^{-2}.s^{-1}$, temperature at 24°C, and position randomized with respect to treatment. Mixed populations of *D. salina* were initiated with 50% of strain A and 50% of strain C, starting at a density of 50,000 cells/ml, and using a different biological replicate (i.e. isogenic population) for each mixture. They were then exposed to 13 cycles of salinity changes, leading to ~180 generations of experimental evolution. Each cycle of salinity change consisted of a step at 2.4M of NaCl (referred to as low salinity; but note that *D. salina* is a halophile, so this salinity is 4 to 5 times higher than seawater), followed by a hyper-osmotic stress where cells were subjected to a steep

salinity rise to 4.0M NaCl (high salinity). Cycles lasted 14 days, and we contrasted two temporal treatments: 4 days at low salinity followed by 10 days at high salinity (hereafter 4-10d cycle), or 7 days at each salinity (hereafter 7-7d cycle). The rationale for doing this is that longer time at high salinity may provide the PCD strain more opportunity to recover from its initial decline during the rebound phase. At each transfer, populations were diluted at a rate of 1/10, and target salinity was achieved by mixing the required volumes of hypo- ([NaCl] = 0 M) and hyper- ([NaCl] = 4.8 M) saline media (Rescan *et al.* 2020), after accounting for dilution of the pre-transfer salinity. At the end of the 13 cycles of the assay, we genetically checked for the presence of both strains within each long-term mixed population (see Supplementary Material).

In addition to these long-term mixed populations, our experiment also included control lines that were subjected to the same salinity treatments for the first 5 cycles. These consisted first of monocultures with only strain A or C, with each replicate consisting of one of the isogenic lines used in the mixtures. These monocultures not only served at controls for putative variation of the decline intensity over cycles (as observed in Zeballos *et al.* 2023), but are also necessary for estimating relative frequencies in the mixtures through the method described below. An additional control consisted of mixtures similar to those in the main experiment, but newly created at each salinity rise by mixing the monocultures at 50%-50%. This allowed assessing whether the population dynamics of long-term mixed populations differed from those of populations with equal proportions of the declining and non-declining strain, thus quantifying the influence of selection (frequency change) on population dynamics. Since the mean generation time of *Dunaliella salina* is ~1 day (Ben-Amotz *et al.* 2009), the first five cycles (with the control lines) corresponded to ~70 generations.

Population density measures

Since our interest is in demographic dynamics following each hyper-osmotic shock, we measured population density daily in the high salinity steps (except days 5 and 6) for the first

five cycles (Fig. 1A) and the two last cycles. In contrast in the low salinity steps, we only measured population densities 1 hour after the salinity transfer to check the dilution rate, and at the end of the step (i.e. on day 4 or day 7 depending on the temporal treatment) to predict the next initial density (if no decline occurred) and calculate the culture volumes required to start the control mixtures at 50,000 cells/ml at the next salinity transfer. Densities measurement pattern for cycles 6 to 11 is explained in Supplementary Material.

We measured population densities by passing 200 µl samples of each population through a Guava® EasyCyte™ HT cytometer (Luminex Corporation, Texas, USA), with a laser emitting at 488 nm. Cells emits natural fluorescence in red (695/50nm) and yellow (583/26nm) due to their chlorophyll α, allowing discrimination of live *Dunaliella* cells from other particles, as described in Rescan *et al.* (2020) and Zeballos *et al.* (2023). PCD was estimated as the rate of initial population decline during the first day following a hyper-osmotic shock.

Caspase-3-like inhibitor assay

It has been shown that the intensity of decline in strain A can be diminished by an inhibitor of caspase-3-like (Zeballos *et al.* 2023), known to be a key player in the metabolic cascade leading to cell death (Ameisen 2002; Danial & Korsmeyer 2004; Kasuba *et al.* 2015; Slee *et al.* 2001). We therefore investigated how this PCD inhibitor influenced strain frequencies in mixed populations, and the subsequent growth dynamics of the mixtures. Monocultures of both strains were acclimated for 4 days at 2.4M, starting at $N_0 = 100{,}000$ cells/ml. For each of the two strains, we then launched 15 monoculture populations at two initial densities (10 populations at $N_0 = 50{,}000$ cells/ml, and 5 populations at $N_0 = 25{,}000$ cells/ml), and prepared 10 mixed populations of both strains started at $N_0 = 50{,}000$ cells/ml (50%-50% for each strain), in total culture volume of 10ml. The two initial densities of the monocultures were done to match either the total density of mixed populations, or the density of each individual strain therein. We applied 2 inhibitor conditions (with or without PCD inhibitor), reaching a total of 80 flasks. In

the inhibitor treatment, a total number of 500,000 cells per flask were treated with 10 µM Z-VAD(Ome)-FMK (CellSignaling) caspase inhibitor, and incubated in the dark for 30min at 24°C, before being subjected to a hyper-osmotic shock at 4M of NaCl. Population densities were measured 30 min and 2 hours after the hyper-osmotic transfer, and then daily tracked over 10 days. Since the inhibitor is supplied as 1 mg of powder and has been diluted in 213.9 µl of DMSO with membrane penetration action (Jacob, S. W., & Herschler 1986), we also checked that this solvent did not prevent decline of strain A monocultures (see Supplementary Material).

Demographic and competition analysis

Decline intensity

To investigate how populations declined over cycles of salinity fluctuations, we fitted generalised linear models (GLM) on population density one hour after the hyper-osmotic transfer (Fig. 1B). We used cytometer cell count at day 0 as response variable, with a log link function, negative binomial error structure, and log expected initial population density (based on pre-transfer density and the dilution rate) as offset (following Rescan *et al*. 2020, Leung *et al* 2022, Zeballos *et al*. 2023). The fixed effects were the type of culture (monoculture or mixture), temporal treatment, and the number of cycles (either as factor or as continuous variable). We extracted the decline rate from those GLM as minus the linear predictor of the GLM (hence, on the log scale), such that steeper decline is represented by a larger positive value (Zeballos *et al.* 2023), and the standard error is unchanged.

Strain frequencies in mixtures

During the assay, we noticed that we were able to distinguish the two strains by their natural yellow and red fluorescence in most mixed populations. However, the distributions of strains A and C still overlapped to some extent (scatter plots in Fig. S1), so we could not use hand-designed cytometry gates to directly count the numbers of each strain. Instead, we estimated strain frequencies in mixtures using a custom-made maximum likelihood method. We assumed

that the pair of traits (yellow and red fluorescence) followed a bivariate Gaussian distribution in each monoculture, with mean vector μ and covariance matrix Σ specific to each strain. The distribution of these same traits in each mixed population was then treated as a mixture of Gaussians from the corresponding monocultures (sampled on the same day), with frequency p for the declining strain A and 1 - p for the non-declining strain C. As all points were measured independently within each assay, we summed their log-likelihoods, and further transformed frequencies to the logit scale $u = \ln(\frac{p}{1-p})$ to facilitate maximization, leading to

$$lnLik = \sum \log\left(\frac{1}{1+e^{-u}} \times f_A(\mu_A, \Sigma_A) + \frac{e^{-u}}{1+e^{-u}} \times f_C(\mu_C, \Sigma_C)\right). \quad \text{(Eq. 1)}$$

We obtained the estimator of $\hat{u}_i$ by maximizing log-likelihood for each isogenic line i. We also extracted the curvature c_i (hessian matrix) of the log-likelihood function at its maximum to estimate uncertainty as $V(\hat{u}_i) = -1/c_i$, relying the asymptotic normal approximation of likelihood (Bulmer 1979; Strimmer 2019). We then computed the 95% confidence interval endpoints on the logit scale for each estimator $\hat{u}_i$ as

$$CI_{95\%}(u_i) = \left[\hat{u}_i - 1.96\sqrt{V(\hat{u}_i)}; \hat{u}_i + 1.96\sqrt{V(\hat{u}_i)}\right]. \quad \text{(Eq. 2)}$$

Isogenic lines of strains A and C used in this experiment differed in how well they could be distinguished in mixtures (Fig. S1), so the mean frequency p was estimated with variable uncertainties depending on which mixture was used. To correct for this heterogeneity and place more weight on more precise estimates, we used the inverse-variance weighting method, which is commonly used in e.g. meta-analyses (when sample sizes differ across studies) (Borenstein *et al.* 2021), and more generally whenever there are known sources variation in uncertainty across estimates (Marin-Martinez & Sánchez-Meca 2010). Accordingly, the mean $\hat{u}$ over the 10 mixtures of isogenic lines (index i) was obtained for each treatment and measurement day as

$$\hat{u}_{mean} = \frac{\sum_i c_i \times \hat{u}_i(p)}{\sum_i c_i} \quad \text{(Eq. 3)}$$

and the error variance of $\hat{u}_{mean}$ as

$$V(\hat{u}_{mean}) = -\frac{1}{\sum_i c_i}. \quad \text{(Eq. 4)}$$

We then computed the 95% confidence interval endpoints on the logit scale for $\hat{u}_{mean}$ by inserting eqs. (3) and (4) into the eq. (2), leading to

$$CI_{95\%}(u_{mean}) = \left[\hat{u}_{mean} - 1.96\sqrt{V(\hat{u}_{mean})}; \hat{u}_{mean} + 1.96\sqrt{V(\hat{u}_{mean})}\right]. \quad \text{(Eq. 5)}$$

For further analyses, we back-transformed the frequency of A in each replicate to the arithmetic scale using the delta method for bias correction (Ver Hoef 2012) as

$$\hat{p}_i = \frac{1}{1+e^{-\hat{u}_i}} + \frac{V(\hat{u}_i)}{2} \times g''(\hat{u}_i) \quad \text{(Eq. 6)}$$

where

$$g''(\hat{u}_i) = \frac{-e^{\hat{u}_i}\,(e^{\hat{u}_i}-1)}{(1+e^{\hat{u}_i})^3}.$$

is the second derivative of the logistic function (inverse of the logit function). We back transformed the confidence interval from eq. (2) by applying the logistic function to its end points. For the mean frequency over the 10 isogenic lines (in each condition and day, Fig. 2), we also used the delta method by combining eqs. (3) and (4) with eq. (6), leading to

$$\hat{p}_{mean} = \frac{1}{1+e^{-\hat{u}_{mean}}} + \frac{V(\hat{u}_{mean})}{2} \times g''(\hat{u}_{mean}). \quad \text{(Eq. 7)}$$

The confidence interval for the mean frequency was then obtained similarly to for each mixture, by applying the logistic function to its end points obtained with the eq. (5). Finally, the error variance for the mean frequency $\hat{p}_{mean}$ was obtained with the delta method (Ver Hoef 2012) as

$$V(\hat{p}_{mean}) = \frac{e^{2\hat{u}_{mean}}}{(1+e^{\hat{u}_{mean}})^4} \times V(\hat{u}_{mean}). \quad \text{(Eq. 8)}$$

We also applied this method to obtain inferred strain frequencies in mixed populations from the inhibitor assay. We tested the efficiency of our estimation method compared to the use of gates on the cytogram (see Supplementary Material and Fig. S2).

Models of density-dependence and competition

Inferred strain densities in mixtures over the first 5 cycles

One of our major aims is to compare the demography of two strains in monocultures vs mixtures, to investigate how these strains interact, and to what extent the population dynamics in monocultures predict the outcome of competition. More specifically, we wished to understand to what extent *per-capita* growth rates of each strain depended on their own density, and that of their competitor. To that intent, we inferred the densities of each strain in the mixtures as $\hat{p}_i \times N_{tot}$, with $\hat{p}_i$ the estimated frequency of each strain in replicates *i* (as described in the previous section), and N_{tot} the total population density (in cells per ml) measured in the flask. We then computed the mean inferred daily density of strain A in the long-term mixtures over the 5 cycles as

$$N_{A,cyc} = E_{cyc}\left(N_{tot,mean}\hat{p}_{mean}\right) = E_{cyc}\left(N_{tot,mean}\right) \times E_{cyc}(\hat{p}_{mean}), \qquad \text{(Eq. 9)}$$

where E_{cyc} denotes an expectation over cycles, $N_{tot,mean}$ and $\hat{p}_{mean}$ are respectively the total population density and frequency of strain A averaged over the 10 isogenic lines within a cycle, and the second member assumes that $N_{tot,mean}$ and $\hat{p}_{mean}$ are independent across cycles. The density of strain C was obtained similarly as $N_{C,cyc} = E_{cyc}\left(N_{tot,mean}\right) \times (1 - E_{cyc}(\hat{p}_{mean}))$. Accordingly, the error variance of $N_{tot,mean}\hat{p}_{mean}$ over the 10 isogenic lines per condition within a cycle was computed as the variance of the product of two independent random variables,

$$V\left(N_{tot,mean}\hat{p}_{mean}\right) = V\left(N_{tot,mean}\right) \times V(\hat{p}_{mean}) + V\left(N_{tot,mean}\right) \times E(\hat{p}_{mean})^2$$

$$+ V(\hat{p}_{mean}) \times E\left(N_{tot,mean}\right)^2 \qquad \text{(Eq. 10)}$$

We then computed the 95% confidence interval of the inferred densities over the 5 cycles using the law of the total variance, $V_{cyc}\left(N_{A,cyc}\right) = E_{cyc}\left(V\left(N_{tot,mean}\hat{p}_{mean}\right)\right) + \frac{V_{cyc}(E(N_{tot}\hat{p}_{mean}))}{nb\ cycles}$, where E_{cyc} and V_{cyc} denote expectations and variances across cycles, respectively, and similarly for strain C. The average density of strain A across cycles and clone mixtures (eq. 9, with the confidence interval from eq. 10), was then compared to its counterpart from monocultures (Fig. 3).

Accounting for uncertainty in analyses of density dependent competition

We wanted to assess the strength of density dependent competition through the relationship between *per-capita* growth rate (over a short time interval) and population density. However, population densities were estimated with error from small cytometer samples. Estimating the density of each strain in a mixture further required estimating the relative frequency of each strain using our mixture distribution approach (eqs. 1-8). This approach not only involves uncertainty in the estimator $\hat{u}_i$ of logit frequency of strain A, but this uncertainty also differs among mixtures of different clones of strains A and C. To account for all these sources of uncertainty, we simulated 1000 datasets, where the frequency $u_{i,simulated}$ of strain A (on the logit scale) in mixture *i* was randomly sampled from a gaussian distribution with mean $\hat{u}_i$ (the estimator of u_i), and standard deviation $\sqrt{V(u_i)}$. We then back-transformed the strain frequencies to the arithmetic scale using the inverse logit function. We also simulated the total number of cells in mixed populations by sampling from a negative binomial distribution with mean $\widehat{N}_t$ and dispersion parameter = 10 (consistent with estimations from GLMs, e.g. Rescan *et al.* 2020). We then computed the simulated density of each strain in mixed cultures for each simulated dataset, as previously explained. From this, the *per-capita* growth rate per day of strain A in mixed populations (for each simulated dataset) was computed as

$$r_A = \frac{\widehat{N}_{A,t} - \widehat{N}_{A,t-\tau}}{\tau\, \widehat{N}_{A,t-\tau}} \qquad \text{(Eq. 11)}$$

with τ the time interval between successive measurements (mostly 1 day, sometimes 2 or 3 days), and similarly for strain C. We restricted the analysis to times t after day 4 (included) and population densities $\widehat{N}_t >$ 5.10^4 cells/ml for both strains, so as to exclude the initial phase of decline-rebound where the relationships between population growth and size are not driven by density dependence. We also focused only on clone mixtures that allowed for clear distinction of both strains, such that the uncertainty in frequency estimation was low ($CI_{95\%}(u_i)$ width $<$ 0.5 on the logit scale).

Finally, we fitted linear models (LM) with the *per-capita* growth rate as response variable, and the densities $\widehat{N}_{t-\tau}$ of both strains or the total densities in mixtures as fixed effects (see Table 1 for details), on each of the 1000 simulated dataset. We computed overall estimates with standard error and p-values over the 1000 LMs using Rubin's rules (assuming normal distributions) (Rubin 1987). We also computed predictions over the 1000 LMs and combined them to produce an overall fitted line (Miles 2016) (Fig. 4). These linear models correspond to the classic Lotka-Volterra model of linear density-dependent competition, so we could check the coexistence condition (Kot 2001). However, the relationship between the *per-capita* growth rate and population density need not be linear, so we also fitted semi-parametric models (cubic splines) using generalized additive models (GAM) (see Table 1 for formula).

Exponential growth rate in the inhibitor assay

We applied a generalised linear model on population densities (from day 2 to 5) of strain A monocultures in the inhibitor assay, to estimate the growth rate during the exponential phase as in Zeballos *et al.* (2023) (Fig. S7). Here, time was included as a continuous explanatory variable, such that its effect estimated the rate of exponential growth per day (linear trend on the log scale), and interactions of time with the other fixed effects (i.e. inhibitor treatment and

initial density) estimated effects of these factors on the maximal exponential growth. All statistical analyses were performed on Rstudio (R version 4.2.0.) using packages MASS (version 7.3.56) (Venables & Ripley 2002), stats (version 4.2.3), mvtnorm (version 1.1.3), mgcv (version 1.8.33), mice (version 3.14) (Van Buuren & Groothuis-Oudshoorn 2011).

Results

Population decline occurs repeatedly over successive hyper-osmotic shocks

The population dynamics over the first 5 cycles of salinity rise are shown in Fig. 1. Soon after each transfer into hypersaline medium, monocultures of strain A (in red) first declined sharply before rebounding through fast growth, eventually reaching a similar density as monocultures of strain C (which grew exponentially from the start), consistent with results in Zeballos *et al.* (2023). The decline-rebound pattern of strain A was repeated over successive hyper-osmotic shocks, with a decline intensity that actually increased over cycles (number of salinity cycles used as a continuous variable, Table S1, P = 0.044, red line in Fig. 1B). The same pattern was found regardless of the duration of cycles (Fig. 1A & S3A), but the increase in decline intensity over cycles was not significant in the 7-7d treatment (Table S1, P = 0.914). The persistence (or even increase) of decline intensity over cycles indicates that this response is not a mere passive consequence of the elimination of cells in bad condition (Zeballos *et al.* 2023).

We analysed mixed populations comprising both strains, to investigate whether a declining genotype could be maintained in competition with a non-declining one. Based on the results of monocultures (here and in Zeballos *et al.* (2023)), we would predict that the declining strain A would outcompete the non-declining strain, thus leading to an increasing rate of decline over cycles in mixtures. However, population dynamics may be fundamentally different in mixtures, for instance if strain C exhausts resources before A is able to rebound from its initial decline (priority effect (De Meester *et al.* 2016)). Here in the first cycle, the initial decline of

mixtures was intermediate between those of strain A and C monocultures, as expected. Mixed cultures maintained a similar initial decline rate at each hyperosmotic shock (Table S1, P = 0.913), suggesting that no strain was able to fully outcompete the other after 180 days (Fig. 1B).

Strain frequencies fluctuate within a cycle but are stable over cycles

We were able to estimate strain frequency in the mixed populations by taking advantage of their differential yellow and red natural fluorescence, and using the monocultures in the same day as references (Fig. S1). Strain A frequency strongly fluctuated in the days following hyper-osmotic shock, starting very low, before increasing until it became dominant in the mixture at the end of the high salinity step, in almost every cycle (Fig. 2). This pattern is consistent with what could be predicted from the decline-rebound pattern in population density observed in monocultures. In the control mixtures, in which the frequency of strain A was set to ~50% before each hyper-osmotic shock, this frequency started at lower value than in long-term mixtures when first measured in the hypersaline environment (after the onset of decline). This suggests that the proportion of strain A before the hyper-osmotic shock was greater than 50% in the long-term mixtures. We confirmed the stable coexistence of both strains in all long-term mixtures by genetically detecting both strains after 13 salinity shocks, corresponding to ~180 generations (Figs. S5).

Since strain A grows faster than strain C during its rebound phase (Fig. 1A; Zeballos *et al.* 2023), we hypothesized that longer hypersaline phases would leave more time for A to outgrow C in mixed populations, provided that they remain in near-exponential growth. However, the pattern of strain A frequency against time in the 7-7d cycles was similar to that in 4-10d cycles, over the 5 successive cycles (Fig. S3B) as well as in the last two cycles (Fig. S4). This suggests that 7 days were sufficient for strain A to reach high enough frequency at the end of each hypersaline phase to not be outcompeted at the next hyper-osmotic shock. This is also consistent with the fact that this frequency did not change much between days 7 and 10

under 4-10d cycles (Fig. 2), suggesting that differences in growth rates of both strains were no longer significant drivers of selection at this time.

To what extent does demography explain selection?

To investigate how these selective dynamics emerge from demography, we calculated the density of each strain in the mixed populations, by multiplying the estimated frequencies of strains A and C by the total population density. The population dynamics of each strain in mixtures (Fig. 3, dashed lines) was qualitatively consistent with that in monocultures (Fig. 3, solid lines), but starting from lower density, since only half of the population was composed of each strain at the start. In the mixtures, strain A had lower density than strain C just after the hyper-osmotic shock as a consequence of PCD, but its higher exponential growth rate during rebound allowed it to reach higher density at the end of the hypersaline phase (Fig. 3, Fig. S3C). This growth advantage during rebound was more pronounced than expected based on monocultures: in Fig. 3, the dashed red line crosses the dashed black line earlier, and their final difference is larger, than for continuous lines (monocultures). This probably occurs because the density of each strain starts lower in mixtures than in monocultures, allowing growth differences to accrue over a longer exponential phase (Fig. 3, Fig. S3C). However, the outcome of this process should also depend on how density dependence acts within and between strains.

To better understand how the growth of each strain is impacted by both intra and inter-genotype competition in the mixtures, we calculated the sensitivity of their *per-capita* growth rates to population density (Fig. 4, Table S2 for LM 1, see Fig. S6 for 7-7d treatment). We observed a significant negative effect of self-density on the *per-capita* growth rate of each strain (P = 5.34e-08 and P = 2.48e-06, Table S2), as classically expected under negative density dependence (i.e., regulation of population growth). Model that included densities of self and the competitor strain as predictors (LM 1) showed that both strains are more sensitive to their own density than to that of their competitor, but that this is more pronounced for strain A (x4.0

for r_A vs x2.5 for r_C, Table S2). Somewhat surprisingly, a linear model where the growth of strain A depends on the total density (strains A+C) performed poorly (higher AIC for LM 2 in Table 1), contrary to the expectation that for closely related strains, competition should depend on the total number of individuals, regardless their genotype.

The fitted linear model (LM1) corresponds to the classic Lotka-Volterra model of linear density-dependent competition, where the *per-capita* growth rate of the strain A is defined by

$$r_A = a_A - b_A\, N_A - c_A N_C, \qquad \text{(Eq. 12)}$$

with a_A the intercept of the linear model (growth rate of strain A when both strains are at low density), and b_A and c_A the slopes of density dependence relative to self and the competitor, respectively (Table S2). (Exchanging subscripts A and C yields the reciprocal equation for strain C.) In this model, the criterion for coexistence of two types is that each one is able to grow when starting from low density while the other is at its demographic equilibrium at carrying capacity (Kot 2001). In terms of parameters of the statistical model, this translates for the growth rate of strain A to

$$r_A = a_A - c_A \frac{a_C}{b_C} > 0, \qquad \text{(Eq. 13)}$$

where $\frac{a_C}{b_C}$ is the equilibrium population size of strain C in monoculture (satisfying $r_C = a_C - b_C\, N_C = 0$). The reciprocal invasion condition for strain C is $a_C - c_C \frac{a_A}{b_A} > 0$. Here we found $a_A - c_A \frac{a_C}{b_C} = 0.98$ and $a_C - c_C \frac{a_A}{b_A} = 0.67$, so the model predicts coexistence of both species. Furthermore, the equilibrium densities of both strains at the end of the stationary phase can be found by jointly solving for $r_A = 0$ and $r_C = 0$, yielding

$$N_{A,Eq} = \frac{c_A a_C - a_A b_C}{b_A\, b_C - c_A c_C} = 3.51\text{e}05 \text{ cells/ml}$$

$$N_{C,Eq} = \frac{c_C a_A - a_C b_A}{b_A\, b_C - c_A c_C} = 2.63\text{e}05 \text{ cells/ml}$$

using the estimates in Table S2. From this, we expect the relative frequency of strain A at the end of the stationary phase to be 0.57, which is below, but not very different, from the observed frequency at the end of each cycle (Fig. 2; average over 5 first cycles: 0.64). This shows that competition between the strains near the stationary phase maintains their coexistence and stabilizes the frequency strain A over cycles, regardless of the initial decline-rebound demographic pattern.

Although the assumption of linear density dependence is convenient to get simple metrics of competition strength, and corresponds to the classic Lotka-Volterra and logistic models from theoretical population ecology (Kot 2001), it might not be the most realistic model (Fronhofer *et al.* 2023). We thus also tested more flexible models that made fewer assumptions about the shape of density dependence, namely spline smoothers as implemented in generalized additive models (GAM, package mgcv in R). The pooled predictions from the GAMs 1 are shown as continuous lines in Fig. 4, showing patterns that are overall very similar to the LMs, except at the highest densities where precision is low due to the small number of points. Accordingly, the outcome of model comparison is qualitatively consistent with the LMs, in that the best model is the one including densities of both strains as fixed effect rather than total density (GAM 1 vs GAM 2, Table 1) for both strains, but larger differences in AIC are observed when the response variable was r_A rather than r_C.

How does a PCD inhibitor affect competition in mixtures?

To demonstrate the role of programmed cell death (PCD) in these eco-evolutionary dynamics, we applied a caspase-3-like inhibitor to mixed populations composed by 50-50% of each strain just before undergoing hyper-osmotic shock. We estimated strain frequencies using monocultures as references as done above (Figs. S7-S8), and then inferred the density of each

strain in the mixtures (Fig. 5). While the treatment without inhibitor led to a sharp initial decline of strain A as above, no population decline was observed for strain A subjected to PCD inhibitor, confirming that the initial decline was attributable to a form of programmed cell death (as also shown by Zeballos *et al.* 2023). Interestingly, the mean growth rate of populations of strain A that underwent initial decline (without inhibitor) was higher than that of populations that did not decline (with inhibitor), over a similar range of densities (in mixtures compare slopes of red vs dashed red lines between eg days 2 and 5 in Fig. 5; for monocultures see Table S4 P = 3.55e-11). It is noteworthy that the initial density did not affect growth rate during the exponential phase of strain A monocultures without PCD inhibitor (Table S4, P = 0.451), consolidating the idea that the demographic rebound after the decline is not just a density-dependence effect due to relaxed competition. Eventually, strain A in mixtures reached a similar density with and without inhibitor (Fig. 5). The population dynamics of strain C were similar under both conditions, despite its competitor having markedly different responses, supporting the idea that the growth of strain C is little sensitive to presence of the other strain.

Discussion

We explored the relationship between absolute and relative fitness and the links between evolution and demography in response to environmental stress, by investigating the outcome of competition between two strains of *Dunaliella salina*, one of which triggers programmed cell death in response to hyper-osmotic shock. We found that competition at high population densities largely explained stable coexistence over 13 cycles of salinity rises, despite strong fluctuations in strain frequencies within each cycle.

Long-term coexistence of alternative strategies

Based on the competition-relatedness relationship, also known as the limiting similarity hypothesis (Charles 1859; Gause 1934; MacArthur & Levins 1967; Violle *et al.* 2011), we

expected that the two closely-related strains we studied would exert strong competition on each other. This could have led to exclusion of the declining strain over cycles, since it starts growing later and at much lower density following each hyper-osmotic shock. Interestingly, we found that instead of responding to the total population density (Table 1, see AIC for LM 2 and GAM 2), as expected for closely related genotypes, the growth rates of strains A and C were mostly sensitive to their own density. This suggests that these strains have different ecological strategies (e.g. use different resources) in the same environment, as also indicated by their strikingly different demographies (Fig 1A, Fig 3). This weak sensitivity to each other's presence allowed their stable coexistence over 13 cycles of salinity changes (DNA confirmation and Fig. 1B), consistent with the fact that they have been sampled in 1976 from the same brackish site (Ginzburg & Ginzburg 1985). Previous work has shown that strain A is almost neutral against strain C at constant salinity 3.2M NaCl (Rescan *et al.* 2021), but strongly counter-selected at constant 2.4M NaCl (our lower salinity here). Interestingly, although the dynamics of selection is here more complex, owing to the decline rebound dynamics at each salinity rise, the long-term coexistence that we find implies selective near-neutrality across cycles, for a mean salinity of 3.2M NaCl per cycle. Hence, fluctuating and constant salinities with a same mean 3.2M led to similar net selection, but probably for different reasons owing to their different demographic dynamics.

Relative and absolute fitness

Being able to measure relative fitness is a crucial issue in experimental evolution. This can be achieved by transforming one of the genotypes, for instance by introducing a gene for a fluorescent protein such as the Green Fluorescent Protein, to allow distinguishing it in a mixture (Gallet *et al.* 2012). However this may complexify analyses, as it requires taking into account the fitness effect of the fluorescent marker, and its potential epistasis with the causal mutation (Gallet *et al.* 2012). Alternatively, sequencing of natural or introduced markers can be used

(Rescan et al. 2021; Levy et al. 2015). Here, we instead took advantage of the natural fluorescence of pigments to discriminate the two strains in mixtures, and thus estimate their frequencies and relative fitnesses. Our method based on analysis of mixture distributions allowed us to estimate frequencies more precisely, and at much lower cost, than using strain-specific amplicon sequencing (as done in Rescan et al. 2021 for the same strains). This allowed us to increase temporal resolution (daily measurements), thus yielding more insights into the non-trivial eco-evolutionary dynamics in this system. We have shown that the dynamics in monocultures were broadly consistent with those of mixtures (Fig. 3), because mixtures seem mostly driven by intra- rather than inter-strain competition. Hence, absolute fitness in monocultures partly predicted selection in mixtures. On the other hand, selection was strongly density-dependent, such that using exponential growth rates as proxies for fitness would not have been relevant to correctly estimate the net coefficient of selection over a cycle (Chevin 2011). This was true regardless of the type of cycle (Fig. S6), and even though the transfer to the next salinity was achieved before reaching the stationary phase in the 7-7d cycle.

Selection on programmed cell death

Beyond the general goal of understanding how selection emerges from demography, the aim of our competition experiment was also to determine whether, and how, selection can favour programmed cell death (PCD). The distinctive decline-rebound pattern of strain A in response to osmotic shock was entirely removed by exposure to an inhibitor of caspase3-like activity (Fig. 5), confirming that it was a form of PCD (consistent with the results in Zeballos et al. 2023). Our results thus demonstrate that PCD can be maintained by selection against a closely related non-PCD strain over successive osmotic shocks, yielding insights into the demographic underpinnings of this selection. However, the ecological and/or physiological mechanisms behind the decline-rebound pattern observed both in monocultures and in mixtures remain to be elucidated. We proposed three potential hypothesis in Zeballos et al. (2023): an altruistic

substrate release by the dying cells, heterogeneity in cell state, or a trade-off between halotolerance and reproduction. Further investigation of these hypotheses through modelling may help distinguish them, based on the dynamics they predict for monocultures and mixtures.

In conclusion, we presented the first experimental evidence for evolutionary maintenance of programmed cell death in a unicellular organism, over many generations and multiple cycles of inductions by environmental stress. Our ability to distinguish genotypes in mixtures and track their population densities throughout the experiment allowed us to link selection and demography in a non-trivial ecological context, and to demonstrate that competition at high density largely explained long-term coexistence, regardless strong frequency fluctuations within a cycle.

Competing interest: Authors declare no competing interests.

Acknowledgments: We thank D. Destoumieux-Garzon, S. Jacob and P. Van Dooren for discussions.

References

Ameisen, J.C. (2002). On the origin, evolution, and nature of programmed cell death: a timeline of four billion years. *Cell Death Differ.*, 9, 367–393.

Ben-Amotz, A., Polle, J.E.W. & Subba Rao, D.V. (2009). *The Alga Dunaliella Biodiversity, Physiology , Genomics and Biotechnology*.

Bidle, K.D. (2016). Programmed Cell Death in Unicellular Phytoplankton. *Curr. Biol.*, 26, R594–R607.

Borenstein, M., Hedges, L. V, Higgins, J.P.T. & Rothstein, H.R. (2021). *Introduction to meta-analysis*. John Wiley \& Sons.

Bulmer, M.G. (1979). Principles of statistics. Courier Corporation.

Burke, M.K., Dunham, J.P., Shahrestani, P., Thornton, K.R., Rose, M.R. & Long, A.D. (2010). Genome-wide analysis of a long-term evolution experiment with Drosophila. *Nature*, 467, 587–590.

Burny, C., Nolte, V., Dolezal, M. & Schlötterer, C. (2022). Genome-wide selection signatures reveal widespread synergistic effects of two different stressors in Drosophila melanogaster. *Proc. R. Soc. B Biol. Sci.*, 289.

Van Buuren, S. & Groothuis-Oudshoorn, K. (2011). mice: Multivariate imputation by chained equations in R. *J. Stat. Softw.*, 45, 1–67.

Cain, A.J. & Sheppard, P.M. (1954). Natural Selection in Cepaea. *Genetics*, 39, 89–116.

Charles, D. (1859). *On the origin of species*. John Murray, London.

Chevin, L.M. (2011). On measuring selection in experimental evolution. *Biol. Lett.*, 7, 210–213.

Crow, J.F. & Kimura, M. (1970). *An Introduction to Population Genetics*.

Danial, N.N. & Korsmeyer, S.J. (2004). Cell Death: Critical Control Points. *Cell*, 116, 205–219.

Deponte, M. (2008). Programmed cell death in protists. *Biochim. Biophys. Acta*, 1783, 1396–1405.

Durand, P.M., Rashidi, A. & Michod, R.E. (2011). How an organism dies affects the fitness of

its neighbors. *Am. Nat.*, 177, 224–232.

Estrela, S., Libby, E., Van Cleve, J., Débarre, F., Deforet, M., Harcombe, W.R., *et al.* (2019). Environmentally Mediated Social Dilemmas. *Trends Ecol. Evol.*, 34, 6–18.

Fisher R. A. & Ford E. B. (1947). The spread of a gene in natural conditions in a colony of the moth Panaxia dominula L. *Heredity (Edinb).*

Fronhofer, E.A., Govaert, L., O'Connor, M.I., Schreiber, S.J. & Altermatt, F. (2023). The shape of density dependence and the relationship between population growth, intraspecific competition and equilibrium population density. *Oikos*, 1–14.

Gallet, R., Cooper, T.F., Elena, S.F. & Lenormand, T. (2012). Measuring selection coefficients below 10-3: Method, Questions, and Prospects. *Genetics*, 190, 175–186.

Gause, G.F. (1934). Experimental analysis of Vito Volterra's mathematical theory of the struggle for existence. *Science (80-.).*, 79, 16–17.

Ginzburg, M. & Ginzburg, B.Z. (1985). Ion and glycerol concentrations in 12 isolates of Dunaliella. *J. Exp. Bot.*, 36, 1064–1074.

Gomulkiewicz, R. & Holt, R.D. (1995). When does evolution by natural selection prevent extinction? *Evolution (N. Y).*, 49, 201–207.

Hendry, A.P. (2017). *Eco-evolutionary Dynamics*. Princeton University Press.

Ver Hoef, J.M. (2012). Who invented the delta method? *Am. Stat.*, 66, 124–127.

Jacob, S. W., & Herschler, R. (1986). Pharmacology of DMSO. *Cryobiology*, 23(1), 14–27.

De Jong, G. (1994). The Fitness of Fitness Concepts and the Description of Natural Selection. *Q. Rev. Biol.*, 69.

Kasuba, K.C., Vavilala, S.L. & D'Souza, J.S. (2015). Apoptosis-like cell death in unicellular photosynthetic organisms - A review. *Algal Res.*, 12, 126–133.

Kot, M. (2001). *Elements of Mathematical Ecology*. Cambridge University Press.

Lenormand, T., Rode, N., Chevin, L. M., & Rousset, F. (2016). Valeur sélective: définitions, enjeux et mesures. In: *Biologie évolutive*. pp. 655–675.

Lenski, R.E. (1991). Quantifying fitness and gene stability in microorganisms. In: *Biotechnology (Reading, Mass.)*. Butterworth-Heinemann, pp. 173–192.

Lenski, R.E., Rose, M.R., Simpson, S.C. & Tadler, S.C. (1997). Long-term experimental evolution in. *J. Evol. Biol.*, 10, 743.

Leung, C., Grulois, D. & Chevin, L.-M. (2022). Plasticity across levels: relating epigenomic, transcriptomic, and phenotypic responses to osmotic stress in a halotolerant microalga. *Mol. Ecol.*

Levy, S.F., Blundell, J.R., Venkataram, S., Petrov, D.A., Fisher, D.S. & Sherlock, G. (2015). Quantitative evolutionary dynamics using high-resolution lineage tracking. *Nature*, 519, 181–186.

MacArthur, R. & Levins, R. (1967). The limiting similarity, convergence, and divergence of coexisting species. *Am. Nat.*, 101, 377–385.

Marin-Martinez, F. & Sánchez-Meca, J. (2010). Weighting by inverse variance or by sample size in random-effects meta-analysis. *Educ. Psychol. Meas.*, 70, 56–73.

De Meester, L., Vanoverbeke, J., Kilsdonk, L.J. & Urban, M.C. (2016). Evolving Perspectives on Monopolization and Priority Effects. *Trends Ecol. Evol.*, 31, 136–146.

Miles, A. (2016). Obtaining Predictions from Models Fit to Multiply Imputed Data. *Sociol. Methods Res.*, 45, 175–185.

Orellana, M. V, Pang, W.L., Durand, P.M., Whitehead, K. & Baliga, N.S. (2013). A Role for Programmed Cell Death in the Microbial Loop. *PLoS One*, 8, e62595.

Reece, S.E., Pollitt, L.C., Colegrave, N. & Gardner, A. (2011). The meaning of death: Evolution and ecology of apoptosis in protozoan parasites. *PLoS Pathog.*, 7, 1–9.

Rescan, M., Grulois, D., Aboud, E.O., de Villemereuil, P. & Chevin, L.-M. (2021). Predicting population genetic change in an autocorrelated random environment: Insights from a large automated experiment. *PLOS Genet.*, 17, e1009611.

Rescan, M., Grulois, D., Ortega-Aboud, E. & Chevin, L.M. (2020). Phenotypic memory drives population growth and extinction risk in a noisy environment. *Nat. Ecol. Evol.*, 4, 193–201.

Ribeck, N. & Lenski, R.E. (2015). Modeling and quantifying frequency-dependent fitness in microbial populations with cross-feeding interactions. *Evolution (N. Y).*, 69, 1313–1320.

Rubin, D.B. (1987). *Multiple Imputation for Nonresponse in Surveys*. John Wiley.

Slee, E.A., Adrain, C. & Martin, S.J. (2001). Executioner Caspase-3, -6, and -7 Perform Distinct, Non-redundant Roles during the Demolition Phase of Apoptosis. *J. Biol. Chem.*, 276, 7320–7326.

Strimmer, K. (2019). *Statistical Methods: Likelihood, Bayes and Regression*. Available at: https://strimmerlab.github.io/publications/lecture-notes/MATH20802/maximum-likelihood-estimation.html. Last accessed 28 May 2024.

Venables, W.N. & Ripley, B.D. (2002). *Modern Applied Statistics with S*. Springer, New York.

Violle, C., Nemergut, D.R., Pu, Z. & Jiang, L. (2011). Phylogenetic limiting similarity and competitive exclusion. *Ecol. Lett.*, 14, 782–787.

Zeballos, N., Grulois, D., Leung, C. & Chevin, L.-M. (2023). Acceptable loss: Fitness consequences of salinity-induced cell death in a halotolerant microalga. *Am. Nat.*, 201.

Tables

Table 1. Model selection for density dependence, based on linear models (LMs) or generalized additive models' (GAMs). In the GAMs formula, s is a function used in definition of smooth terms. Akaike information criterion was averaged over 1000 LMs (estimated on resimulated datasets to account for uncertainty). The best model based on AIC is shown in bold.

LMs	**Variable response: $r_{strain\ 1}$** **Fixed effects:**	**AIC** $r_{strain\ A}$	AIC $r_{strain\ C}$
Model 1	$N_{strain\ 1,t-\tau} + N_{strain\ 2,t-\tau}$	**432.61**	**442.63**
Model 2	$N_{Total,t-\tau}$	444.18	447.77
GAMs	**Variable response: $r_{strain\ 1}$** **Fixed effects:**	AIC $r_{strain\ A}$	AIC $r_{strain\ C}$
Model 1	$s(N_{strain\ 1,t-\tau}) + s(N_{strain\ 2,t-\tau})$	**418.85**	**433.06**
Model 2	$N_{Total,t-\tau}$	438.79	445.99

Figures

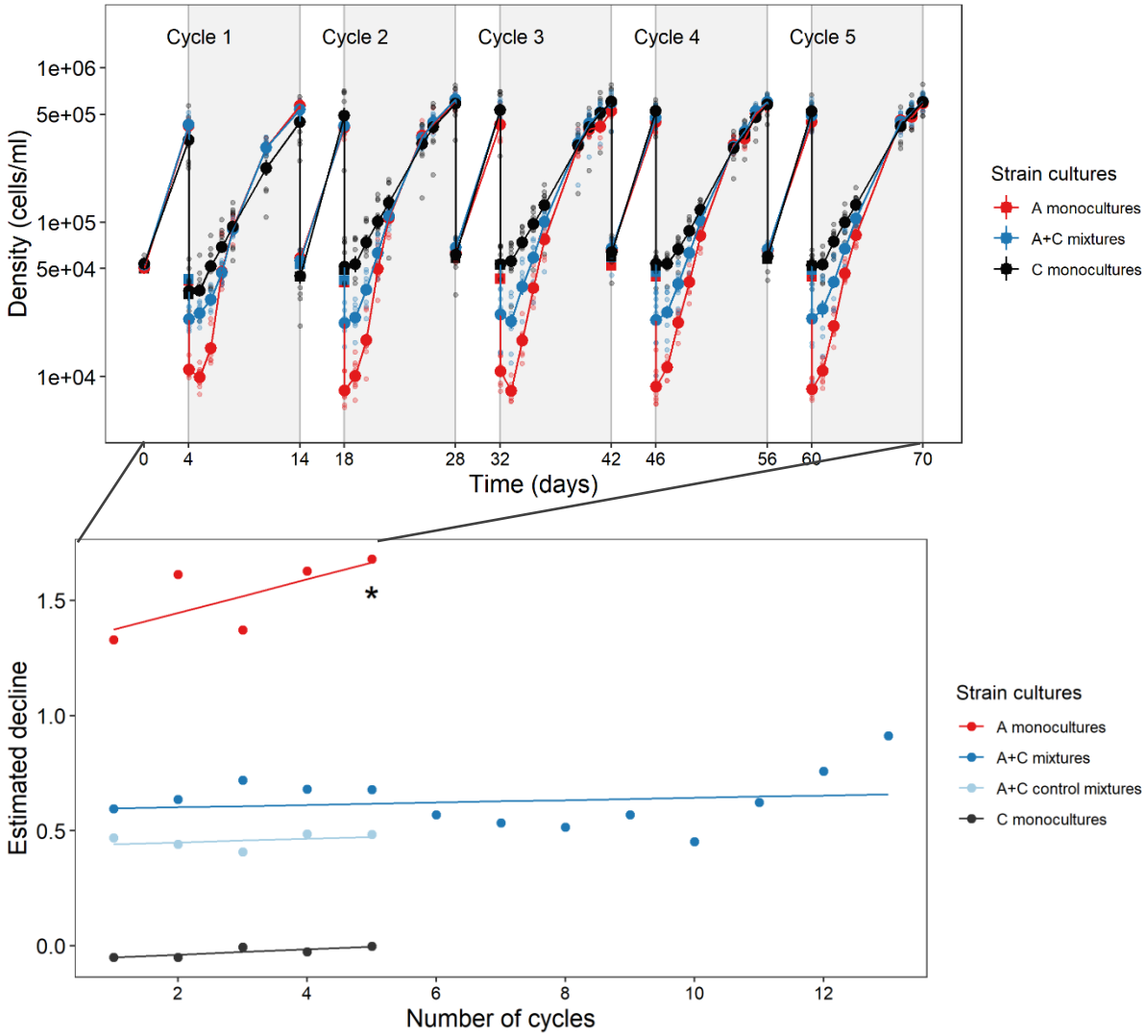

Figure 1. Demographic responses to successive salinity rises. (A) Populations densities over the first five salinity cycles are shown for monocultures of strain A (red) and strain C (black), and long-term mixtures of A and C (blue). Small dots represent biological replicates (specific isogenic lines of each strain, and mixtures thereof), while large dots represent means over replicates (with SE not visible). Grey backgrounds correspond to the high salinity steps in a given cycle. (B) The estimated rate of initial decline one hour after the hyper-osmotic shock is shown over cycles, based on GLMs where the number of cycles was treated either as factor (dots), or as a continuous variable (lines). The star denotes p-value <0.1 for the slope of decline rate against cycle number.

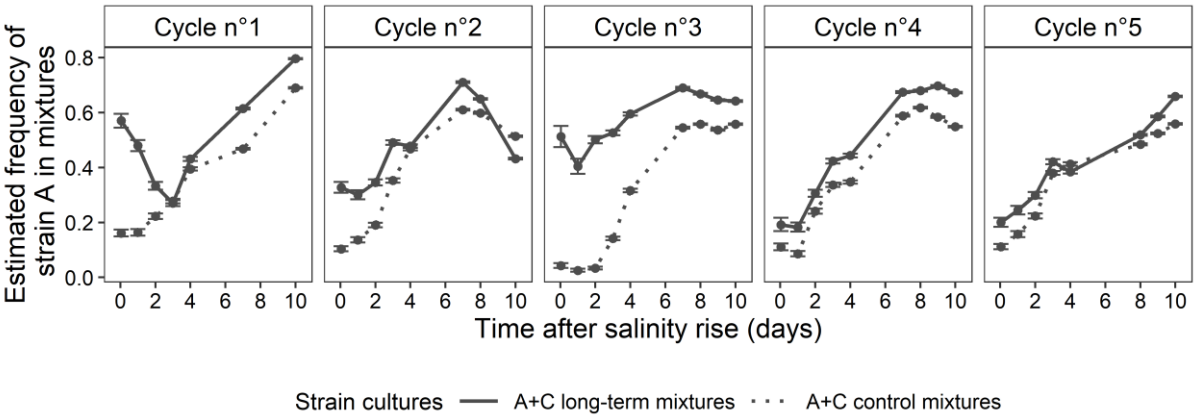

Figure 2. Frequency of declining strain over 5 successive salinity rises. The proportion of strain A in mixed populations, as estimated from the cytometric traits of cells, is shown against time for long-term mixtures (solid lines), and control mixtures (dotted lines) that were freshly composed by mixing 50-50% of each strain before each salinity rise. Means and 95% confidence intervals were obtained on the logit scale by inverse-variance weighting over the 10 population lines, to account for the variable uncertainty of estimates among biological replicates (isogenic lines of each strain), and back-transformed to the arithmetic scale using the delta method.

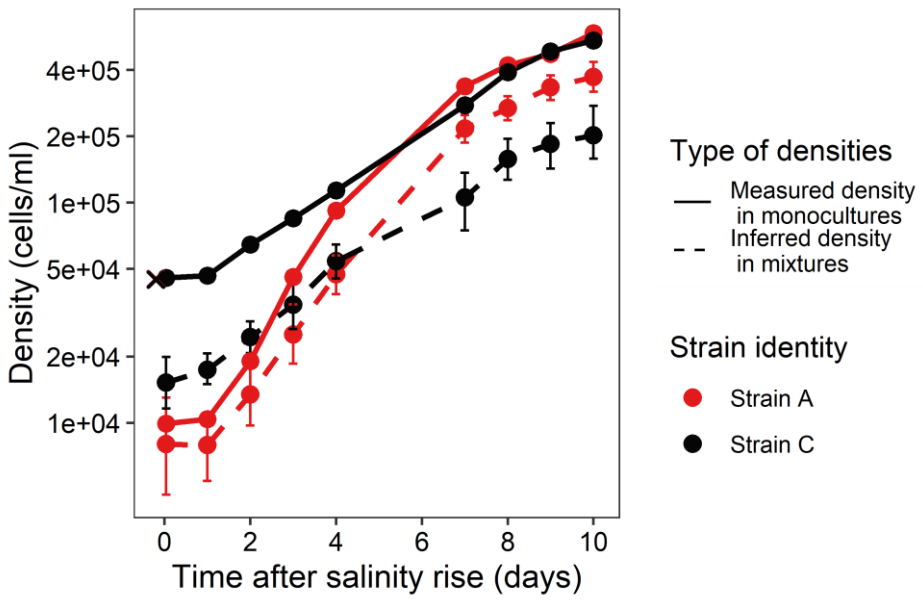

Figure 3. Growth rates in monocultures versus mixtures. Mean population densities across replicates in monocultures (solid lines; direct measurements), and long-term mixtures (dashed lines; inferred from the estimate of relative frequencies), averaged over the first 5 high salinity steps, are shown for the 4-10d fluctuation cycle. For the monocultures, we computed the mean and standard error (not visible) over 10 isogenic lines. For the mixtures, we used inverse-variance-weighted mean (eq. 9, computed with the delta method) and 95% confidence interval, to account for variable precision in estimation of strain A frequency among biological replicates. The crosses at time 0 (overlapping for red and black) correspond to the expected initial densities for monocultures, based on the known density before the 10% dilution.

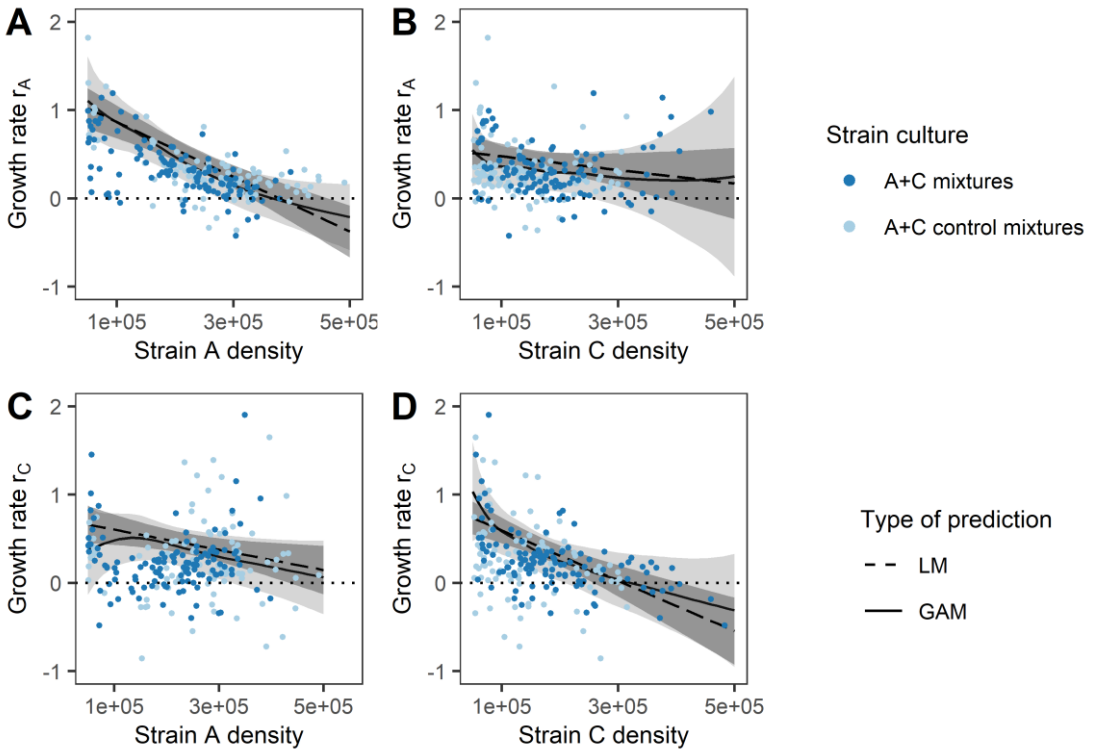

Figure 4. Intra- and inter-strain competition and population growth. The *per-capita* growth rate of strain A (A-B) or strain C (C-D) is shown against the density of strain A (A, C) or strain C (B, D), in the 4-10d fluctuation cycle. Each point corresponds to the *per-capita* growth rate over the interval between two subsequent population measurements. The predictions from linear models (LM1, straight dashed lines and dark gray 95% CI) and generalized additive models (GAM1, continuous lines and light gray 95% CI) are also shown, pooling estimates from 1000 resimulated datasets to account for uncertainty in *r* and *N*, and setting the density of the strain not represented in the x-axis to its median. We set the y-axis maximum to 2 for the sake of graphical clarity, which led to removing 2 dots in A-B (r_A = 2.3; 3.9) and 1 in C-D (r_C =2.4).

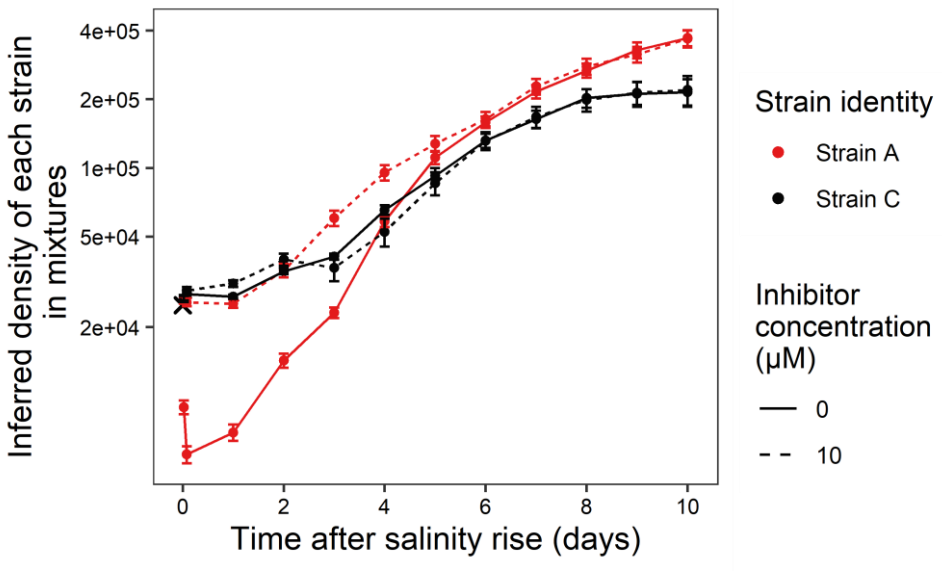

Figure 5. Impact of a programmed cell death inhibitor on growth in competition. Densities of each strain (colours) in the mixtures are shown under different doses of PCD inhibitor (line type), against days following a single salinity rise. Transfers occur at day 0, and the first measurements were made 30 min, and then 2 hours after the transfer. The cross corresponds to the expected initial density. Filled symbols are weighted averages (accounting for uncertainty in distinguishing the strains in mixtures) over 10 replicates, and error bars indicate confidence interval at 95.